AIAA Guidance, Navigation, and Control Conference
13 - 16 August 2012, Minneapolis, Minnesota

AIAA 2012-4601

Retrospective-Cost-Based Adaptive State Estimation and Input Reconstruction for the Global Ionosphere-Thermosphere Model

Kshitij Agarwal*, Asad A. Ali†, Anthony M. D'Amato‡, Aaron J. Ridley§,
and Dennis S. Bernstein¶

University of Michigan, 1320 Beal Ave., Ann Arbor, MI 48109

We consider the problem of estimating the unknown solar driver F10.7 and physical states in the ionosphere and thermosphere using retrospective cost adaptive state estimation (RCASE). We interface RCASE with the Global Ionosphere Thermosphere Model (GITM) to demonstrate state estimation and F10.7 input reconstruction. We further examine the various factors that affect F10.7 estimation including saturation limits, initial estimates, and RCASE tuning parameters.

I. Introduction

State estimation techniques, such as the Kalman filter and its variants, use measurements to recursively refine state estimates. The input to the system is typically modeled as a combination of an unknown stochastic signal and a known deterministic signal. The deterministic signal is injected numerically into the observer which enhances the accuracy of the state estimation. In practice, however, the deterministic input may not be known, and treating this signal as part of the stochastic input may yield poor state estimates due to the modeling mismatch. Consequently, extensive research has been devoted to developing extensions of the Kalman filter that are either insensitive to knowledge of the deterministic input or that attempt to estimate this signal in addition to the states. These techniques are referred to as unbiased Kalman filters, unknown input observers, and state estimators with input reconstruction [1–8].

For many systems, the response is primarily due to the input since the effect of the initial state decays, and the asymptotic response is governed entirely by the forcing. In the linear case, systems with this property are asymptotically stable. In the nonlinear case, these systems are called *incrementally stable* or *contractive*, and the relevant phenomenon is called *entrainment* [9–11]. The phenomenon of entrainment suggests that, atleast in some cases, the accuracy of state estimation may depend strongly on the ability to perform input reconstruction.

The present paper is concerned with the modeling and prediction of space weather effects. In the near-Earth environment, the effects of space weather are manifested by the properties of the ionosphere and thermosphere, which have a strong effect on satellite drag and radio propagation. The ionosphere and thermosphere are strongly driven by the Sun. In particular, the extreme ultraviolet radiation produces photo-ionization, which in turn, through chemistry and heating, drives the properties of the ionosphere and

*Graduate Student, Aerospace Engineering Department
†Graduate Student, Aerospace Engineering Department
‡NASA GSRP Fellow, Aerospace Engineering Department
§Professor, Atmospheric Oceanic and Space Sciences
¶Professor, Aerospace Engineering Department

thermosphere. Since a significant portion of the EUV and X-ray radiation is absorbed in the atmosphere, it is not possible to measure the flux from the ground. Instead, a proxy is used. The flux solar irradiance at a wavelength of 10.7 cm (F10.7) can be measured on the ground and used to estimate the solar spectrum in the 0-150 nm range. The unit of F10.7 is $10^{-22}W/Hz/m^2$ which is equivalent to 1 solar flux unit. The problem with this technique is that the F10.7 does not have a one-to-one correlation with each of the wavelengths in the EUV band, and thus the measured F10.7 is often a misrepresentation of the true spectrum. An ultimate goal would be to estimate the true flux in the various EUV wavelength bins, but an intermediate goal is to estimate the F10.7 that best characterizes the present thermosphere and ionosphere. This study attempts to specify the F10.7 based on measurements from a simulation of the atmosphere. These estimates can then be used to better specify the current state of the ionosphere and thermosphere globally and possibly predict its future evolution. This is a problem of state estimation with input reconstruction.

The starting point for the present paper is the retrospective cost adaptive state estimation (RCASE) technique of [13]. RCASE uses an adaptive state estimation and input reconstruction technique to asymptotically estimate the unknown input to the system. A regularization technique is used in the case that the transfer function from the disturbance to the measurement is nonmiminum phase, in which case the standard Kalman filter is unable to achieve asymptotically exact estimation. A useful feature of RCASE is that, for nonlinear systems, no explicit nonlinear or linearized model is required. Consequently, RCASE is applicable to large scale computational models, as described below.

The goal of the present paper is to investigate the performance of the adaptive state estimation technique of [13] for estimating F10.7. The basis for this investigation is the Global Ionosphere-Thermosphere (GITM) code [14–18]. GITM is a three-dimensional spherical (global Earth) code that solves the Navier-Stokes equations for the thermosphere. GITM is different from other models of the atmosphere [14–16] in that it solves the full vertical momentum equation instead of assuming that the atmosphere is in hydrostatic equilibrium, where the pressure gradient is balanced by gravity. While this assumption is valid for the majority of the atmosphere, in the auroral zone, where significant energy is dumped into the thermosphere on short time scales, vertical accelerations often occur. This heating causes strong vertical winds that can significantly lift the atmosphere [17]. The grid structure within GITM is fully parallel and covers the entire surface of the Earth by using a block-based two-dimensional domain decomposition in the horizontal coordinates [18]. The number of latitude and longitude blocks can be specified at run time in order to modify the horizontal resolution. GITM has been run on up to 256 processors with a resolution as fine as 0.31 latitude by 2.5 longitude over the entire globe with 50 vertical levels, covering a vertical domain from 100 km to roughly 600 km. This flexibility can be used to validate consistency by running model refinement at various levels of resolution.

The contents of this paper are as follows. In Section II, we give a problem formulation for nonlinear state estimation and input reconstruction. In Section III we discuss the retrospective cost based state estimation and input reconstruction algorithm that we use to estimate the solar drivers, specifically, F107 and the states in the GITM model. Next, in Section IV, we describe the adaptive feedback construction and update mechanism of RCASE. Finally, in Section V we report the results of numerical experiments where RCASE is used with simulated data from GITM to estimate F10.7.

II. Problem Formulation

Consider the MIMO discrete-time system

$$x(k+1) = f(x(k)) + g(u(k)), \tag{1}$$
$$y(k) = h(x(k)), \tag{2}$$
$$\tag{3}$$

where $x(k) \in \mathbb{R}^n$, $y(k) \in \mathbb{R}^p$, $u(k) \in \mathbb{R}^m$, and $k \geq 0$. The system (1)–(2) represents the truth GITM model.

Next, we construct the estimator system based on a copy of the GITM model

$$\hat{x}(k+1) = f(\hat{x}(k)) + g(\hat{u}(k)), \tag{4}$$
$$\hat{y}(k) = h(\hat{x}(k)), \tag{5}$$
$$\hat{y}_0(k) = h_0(\hat{x}(k)), \tag{6}$$
$$z(k) = \hat{y}(k) - y(k), \tag{7}$$

where $\hat{x}(k) \in \mathbb{R}^n$ is the estimated state, $\hat{y}(k) \in \mathbb{R}^p$ is the estimated output, $\hat{u}(k) \in \mathbb{R}^m$ is the estimated driver, $z(k) \in \mathbb{R}^p$ is a performance variable, and $\hat{y}_0(k) \in \mathbb{R}^{l_{y_0}}$ is an internal signal specified in Section IV. Furthermore, we assume that $\hat{u}(k)$ is the output of the strictly proper adaptive feedback system of order n_c, with input $\hat{y}_0(k)$, given by

$$\hat{u}(k) = \sum_{i=1}^{n_c} M_i(k)\hat{u}(k-i) + \sum_{i=1}^{n_c} N_i(k)\hat{y}_0(k-i), \tag{8}$$

where, for all $i = 1, \ldots, n_c$, $M_i(k) \in \mathbb{R}^{m\times m}$ and $N_i(k) \in \mathbb{R}^{m\times l_{y_0}}$. The goal is to update $M_{i,k}$ and $N_{i,k}$ using the measured output error $z(k)$. Figure 1 shows the adaptive estimator structure.

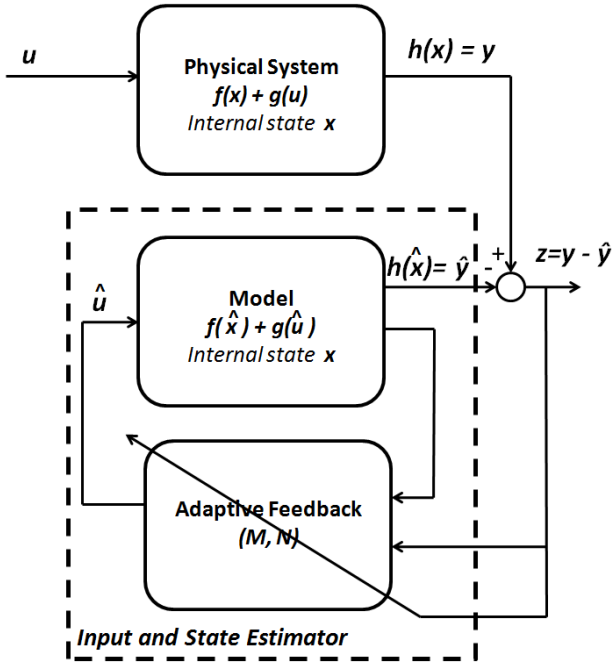

Figure 1. Adaptive State Estimation and Input Reconstruction Architecture

III. Input Reconstruction and State Estimation Using a Retrospective Cost Function

Let A, B, and C denote the Jacobians of f, g_u, and h, respectively. For $i \geq 1$, define the Markov parameter H_i of (A, B, C) given by

$$H_i \triangleq E_1 A^{i-1} B. \tag{9}$$

For example, $H_1 = E_1B$ and $H_2 = E_1AB$. Let r be a positive integer. Then, for all $k \geq r$,

$$\hat{x}(k) = A^r\hat{x}(k-r) + \sum_{i=1}^{r} A^{i-1}B\hat{u}(k-i), \tag{10}$$

and thus

$$z(k) = E_1A^r\hat{x}(k-r) + y(k) + \bar{H}\hat{\bar{U}}(k-1), \tag{11}$$

where

$$\bar{H} \triangleq \left[\begin{array}{ccc} H_1 & \cdots & H_r \end{array} \right] \in \mathbb{R}^{p\times rm}$$

and

$$\hat{\bar{U}}(k-1) \triangleq \left[\begin{array}{c} \hat{u}(k-1) \\ \vdots \\ \hat{u}(k-r) \end{array} \right].$$

Next, we rearrange the columns of $\bar{H}$ and the components of $\hat{\bar{U}}(k-1)$ and partition the resulting matrix and vector so that

$$\bar{H}\hat{\bar{U}}(k-1) = \mathcal{H}'\hat{U}'(k-1) + \mathcal{H}\hat{U}(k-1), \tag{12}$$

where $\mathcal{H}' \in \mathbb{R}^{p\times(rm-l_{\hat{U}})}$, $\mathcal{H} \in \mathbb{R}^{p\times l_{\hat{U}}}$, $\hat{U}'(k-1) \in \mathbb{R}^{rm-l_{\hat{U}}}$, and $\hat{U}(k-1) \in \mathbb{R}^{l_{\hat{U}}}$. Then, we can rewrite (11) as

$$z(k) = \mathcal{S}(k) + \mathcal{H}\hat{U}(k-1), \tag{13}$$

where

$$\mathcal{S}(k) \triangleq E_1A^r\hat{x}(k-r) + y(k) + \mathcal{H}'\hat{U}'(k-1). \tag{14}$$

Note that the decomposition of $\bar{H}\hat{\bar{U}}(k-1)$ in (12) is not unique. Let s be a positive integer. Then for $i = 1, \ldots, s$, we replace $\mathcal{H}$, $\hat{U}(k-1)$, $\mathcal{H}'$, and $\hat{U}'(k-1)$ in (12) with $\mathcal{H}_j \in \mathbb{R}^{p\times l_{\hat{U}_j}}$, $\hat{U}_j(k-1) \in \mathbb{R}^{l_{\hat{U}_j}}$, $\mathcal{H}'_j \in \mathbb{R}^{p\times(rm-l_{\hat{U}_j})}$, and $\hat{U}'_j(k-1) \in \mathbb{R}^{rm-l_{\hat{U}_j}}$, respectively, such that (12) becomes

$$\bar{H}\hat{\bar{U}}(k-1) = \mathcal{H}'_j\hat{U}'_j(k-1) + \mathcal{H}_j\hat{U}_j(k-1). \tag{15}$$

Therefore, for $j = 1, \ldots, s$, we can rewrite (13) as

$$z(k) = \mathcal{S}_j(k) + \mathcal{H}_j\hat{U}_j(k-1), \tag{16}$$

where

$$\mathcal{S}_j(k) \triangleq E_1A^r\hat{x}(k-r) + y(k) + \mathcal{H}'_j\hat{U}'_j(k-1). \tag{17}$$

Next, let $0 \leq k_1 \leq k_2 \leq \cdots \leq k_s$. Replacing k by $k-k_j$ in (16) yields

$$z(k-k_j) = \mathcal{S}_j(k-k_j) + \mathcal{H}_j\hat{U}_j(k-k_j-1). \tag{18}$$

Now, by stacking $z(k-k_1), \ldots, z(k-k_s)$, we define the *extended performance*

$$Z(k) \triangleq \left[\begin{array}{c} z(k-k_1) \\ \vdots \\ z(k-k_s) \end{array} \right] \in \mathbb{R}^{sp}. \tag{19}$$

Therefore,

$$Z(k) \triangleq \tilde{\mathcal{S}}(k) + \tilde{\mathcal{H}}\hat{\tilde{U}}(k-1), \tag{20}$$

where

$$\tilde{\mathcal{S}}(k) \triangleq \begin{bmatrix} \mathcal{S}_1(k-k_1) \\ \vdots \\ \mathcal{S}_s(k-k_s) \end{bmatrix} \in \mathbb{R}^{sp} \tag{21}$$

and $\hat{\tilde{U}}(k-1)$ has the form

$$\hat{\tilde{U}}(k-1) \triangleq \begin{bmatrix} \hat{u}(k-q_1) \\ \vdots \\ \hat{u}(k-q_g) \end{bmatrix} \in \mathbb{R}^{gm}, \tag{22}$$

where $k_1 \leq q_1 < q_2 < \cdots < q_g \leq k_s + r$. The vector $\hat{\tilde{U}}(k-1)$ is formed by stacking $\hat{U}_1(k-k_1-1), \ldots, \hat{U}_s(k-k_s-1)$ and removing copies of repeated components, and $\tilde{\mathcal{H}} \in \mathbb{R}^{sp \times gm}$ is constructed according to the structure of $\hat{\tilde{U}}(k-1)$.

Next, we define the *retrospective performance*

$$\hat{z}(k-k_j) \triangleq \mathcal{S}_j(k-k_j) + \mathcal{H}_j U_j^*(k-k_j-1), \tag{23}$$

where the past input estimates $\hat{U}_j(k-k_j-1)$ in (18) are replaced by the retrospectively optimized input estimates $U_j^*(k-k_j-1)$, which are determined below. In analogy with (19), the *extended retrospective performance* is defined as

$$\hat{Z}(k) \triangleq \begin{bmatrix} \hat{z}(k-k_1) \\ \vdots \\ \hat{z}(k-k_s) \end{bmatrix} \in \mathbb{R}^{sp} \tag{24}$$

and thus is given by

$$\hat{Z}(k) = \tilde{\mathcal{S}}(k) + \tilde{\mathcal{H}}\tilde{U}^*(k-1), \tag{25}$$

where the components of $\tilde{U}^*(k-1) \in \mathbb{R}^{l_{\hat{U}}}$ are the components of ${U^*}_1(k-k_1-1), \ldots, U_s^*(k-k_s-1)$ ordered in the same way as the components of $\hat{\tilde{U}}(k-1)$. Subtracting (20) from (25) yields

$$\hat{Z}(k) = Z(k) - \tilde{\mathcal{H}}\hat{\tilde{U}}(k-1) + \tilde{\mathcal{H}}\tilde{U}^*(k-1). \tag{26}$$

Finally, we define the *retrospective cost function*

$$J(\tilde{U}^*(k-1), k) \triangleq \hat{Z}^{\mathrm{T}}(k) R_1(k) \hat{Z}(k) + \eta(k) \tilde{U}^{*\mathrm{T}}(k-1) R_2(k) \tilde{U}^*(k-1), \tag{27}$$

where $R_1(k) \in \mathbb{R}^{ps \times ps}$ is a positive-definite performance weighting, $R_2(k) \in \mathbb{R}^{gm \times gm}$ is a positive-definite input estimate weighting, and $\eta(k) \geq 0$ is a regularization weighting. The goal is to determine retrospective input estimates $\tilde{U}^*(k-1)$ that would have provided better performance than the estimated inputs $\hat{U}(k-1)$ that were applied to the system. The retrospectively optimized estimated input values $\tilde{U}^*(k-1)$ are then used to update the controller. Substituting (26) into (27) yields

$$J(\tilde{U}^*(k-1), k) = \tilde{U}^{*\mathrm{T}}(k-1) \mathcal{A}(k) \tilde{U}^*(k-1) + \tilde{U}^{*\mathrm{T}}(k-1) \mathcal{B}^{\mathrm{T}}(k) + \mathcal{C}(k), \tag{28}$$

where

$$\mathcal{A}(k) \triangleq \tilde{\mathcal{H}}^{\mathrm{T}} R_1(k) \tilde{\mathcal{H}} + \eta(k) R_2(k), \tag{29}$$

$$\mathcal{B}(k) \triangleq 2\tilde{\mathcal{H}}^{\mathrm{T}} R_1(k)[Z(k) - \tilde{\mathcal{H}}\hat{\tilde{U}}(k-1)], \tag{30}$$

$$\mathcal{C}(k) \triangleq Z^{\mathrm{T}}(k) R_1(k) Z(k) - 2Z^{\mathrm{T}}(k) R_1(k) \tilde{\mathcal{H}} \hat{\tilde{U}}(k-1) + \hat{\tilde{U}}^{\mathrm{T}}(k-1) \tilde{\mathcal{H}}^{\mathrm{T}} R_1(k) \tilde{\mathcal{H}} \hat{\tilde{U}}(k-1). \tag{31}$$

If either $\tilde{\mathcal{H}}$ has full column rank or $\eta(k) > 0$, then $\mathcal{A}(k)$ is positive definite. In this case, $J(\tilde{U}^*(k-1), k)$ has the unique global minimizer

$$\hat{\tilde{U}}(k-1) = -\frac{1}{2} \mathcal{A}^{-1}(k) \mathcal{B}(k), \tag{32}$$

which is the retrospectively optimized estimated inputs.

The regularization weighting $\eta(k)$ can be used to bound the retrospectively optimized estimated inputs $\tilde{U}^*(k-1)$ and thus indirectly bound the estimated inputs $\hat{\tilde{U}}(k)$. For example, $\eta(k)$ may be performance based

$$\eta(k) = \eta_0(k) ||Z(k)||_2^2 \tag{33}$$

or error based

$$\eta(k) = \eta_0(k) ||\tilde{U}^*(k-2) - \hat{\tilde{U}}(k-2)||_2^2, \tag{34}$$

where $\eta_0(k) \geq 0$. Alternatively, the retrospectively optimized inputs can be bounded directly by using a saturation function, where $\eta(k) \equiv 0$ in (29) and (32) is replaced by

$$\tilde{U}^*(k-1) \triangleq \mathrm{sat}_{[a,b]}[-\frac{1}{2} \mathcal{A}^{-1}(k) \mathcal{B}(k)], \tag{35}$$

where $\mathrm{sat}_{[a,b]}(\zeta)$ is the component-wise saturation function defined for scalar arguments by

$$\mathrm{sat}_{[a,b]}(\zeta) \triangleq \begin{cases} b, & \text{if } \zeta \geq b, \\ \zeta, & \text{if } a < \zeta < b, \\ a & \text{if } \zeta \leq a, \end{cases} \tag{36}$$

where $a < b$ are the component-wise saturation levels.

IV. Adaptive Feedback Construction and Update

The estimated input $\hat{u}(k)$ given by (8) can be expressed as

$$\hat{u}(k) = \theta(k) \phi(k-1), \tag{37}$$

where

$$\theta(k) \triangleq [M_1(k) \ \cdots \ M_{n_c}(k) \ N_1(k) \ \cdots \ N_{n_c}(k)] \in \mathbb{R}^{m \times n_c(m+l_{y_0})} \tag{38}$$

and

$$\phi(k-1) \triangleq \begin{bmatrix} \hat{u}(k-1) \\ \vdots \\ \hat{u}(k-n_c) \\ \hat{y}_0(k-1) \\ \vdots \\ \hat{y}_0(k-n_c) \end{bmatrix} \in \mathbb{R}^{n_c(m+l_{y_0})}. \tag{39}$$

IV.A. Recursive Least Squares Update of $\theta(k)$

We define the cumulative cost function

$$J_{\mathrm{R}}(\theta(k)) \triangleq \sum_{i=q_g+1}^{k} \lambda^{k-i}\|\phi^{\mathrm{T}}(i-q_g-1)\theta^{\mathrm{T}}(k) - u^{*\mathrm{T}}(i-q_g)\|^2 + \lambda^k(\theta(k)-\theta(0))P^{-1}(0)(\theta(k)-\theta(0))^{\mathrm{T}}, \quad (40)$$

where $\|\cdot\|$ is the Euclidean norm and, for some $\varepsilon \in (0,1)$, $\lambda(k) \in (\varepsilon, 1]$ is the forgetting factor, and $P(0) \in \mathbb{R}^{n_c(m+l_{y_0})\times n_c(m+l_{y_0})}$ is the initial covariance matrix. Minimizing (40) yields

$$\begin{aligned}\theta^{\mathrm{T}}(k) \triangleq \theta^{\mathrm{T}}(k-1) &+ \beta(k)P(k-1)\phi(k-q_g-1)[\phi^{\mathrm{T}}(k-q_g-1)P(k-1)\phi(k-q_g-1)+\lambda(k)]^{-1} \\ &\cdot [\theta(k-1)\phi(k-q_g-1) - u^*(k-q_g)]^{\mathrm{T}}, \end{aligned} \quad (41)$$

where $\beta(k)$ is either 0 or 1. When $\beta(k) = 1$, the controller is allowed to adapt, whereas, when $\beta(k) = 0$, the adaptation is off. The covariance matrix is updated by

$$\begin{aligned}P(k) \triangleq (1-\beta(k))P(k-1) &+ \beta(k)\lambda^{-1}(k)P(k-1) - \beta(k)\lambda^{-1}(k)P(k-1)\phi(k-q_g-1) \\ &\cdot [\phi^{\mathrm{T}}(k-q_g-1)P(k-1)\phi(k-q_g-1)+\lambda(k)]^{-1}\phi^{\mathrm{T}}(k-q_g-1)P(k-1). \end{aligned} \quad (42)$$

We initialize the covariance matrix as $P(0) = \gamma I$, where $\gamma > 0$. Furthermore, the updates (41) and (42) are based on the g^{th} component of $\tilde{U}^*(k-1)$. However any or all of the components of $\tilde{U}^*(k-1)$ may be used in the update of $\theta(k)$ and $P(k)$.

V. Application to F10.7 Estimation

In this section, we consider the problem of estimating F10.7 and physical states in the ionosphere-thermosphere using mass-density measurements obtained from GITM. We define the "truth model" as GITM with the true value of F10.7=150. We use this truth model to simulate the chemistry and fluid dynamics in a one-dimensional column in the ionosphere-thermosphere and generate mass-density measurements at an altitude of 400 km above the earth. This mass-density measurement is the "truth data", which we label as $y_0(k)$. We also generate measurements of temperature and velocity at the same location and altitude of 400 km, which represent two physical states of the system. Next, we assume that the F10.7 is unknown. We use RCASE to estimate the true value of F10.7 at each time step, and then use the estimate as an input to a copy of GITM, which we refer to as the "data assimilation model". The time step is fixed at 3 seconds in all simulations. We also define the performance variable as

$$z(k) \triangleq \hat{y}_0(k) - y_0(k), \quad (43)$$

which represents the difference between measured and estimated neutral densities at 400 km above the Earth's surface.

First, we take an initial estimate of F10.7=140, and set saturation limits on F10.7 between 130 and 170. We set the RCASE parameters $n_c = 1$, $\tilde{H} = 100$, $\bar{\eta} = 0$, and $\gamma = 0.01$. Each simulation begins at midnight. Since F10.7 has a more significant effect on the atmosphere during daytime, RCASE is turned on after 3000 steps to ensure that the estimation process begins during daytime. Figure 2 shows the performance $z(k)$, and Figure 3 shows the F10.7 estimate. It can be seen that the true value of F10.7 is estimated in less than one simulated day. Figure 4 shows the estimated θ, and Figure 5 shows the output from the truth model $y_0(k)$ and the output $\hat{y}_0(k)$ from the data assimilation model. Furthermore, temperature and velocity at the same altitude are shown in Figures 6 - 7, which converge to their true values in less than a day as well.

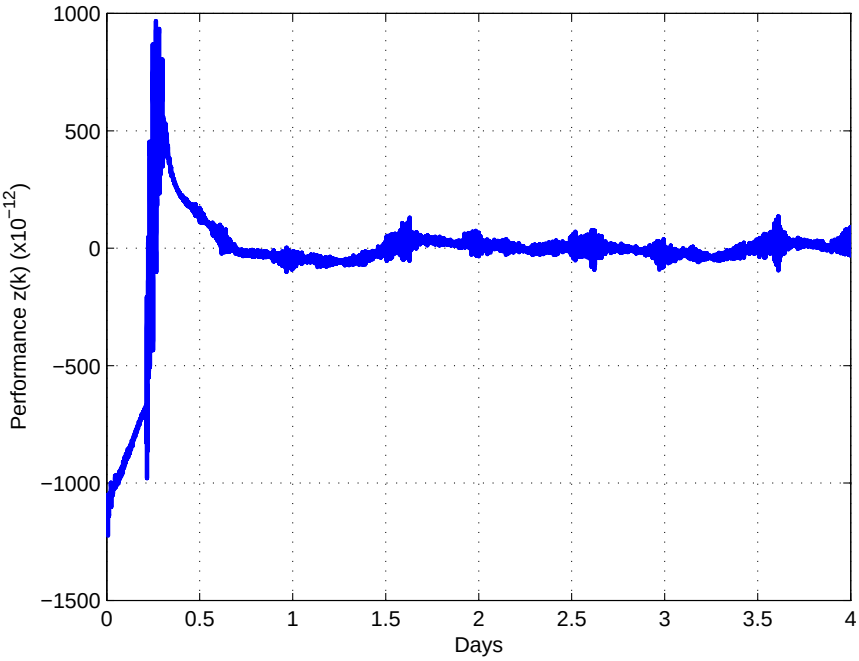

Figure 2. Performance $z(k)$ given by the error in the mass density estimates for the case where the initial guess of F10.7 is 140 and the saturation limits for the simulation are set to 130/170.

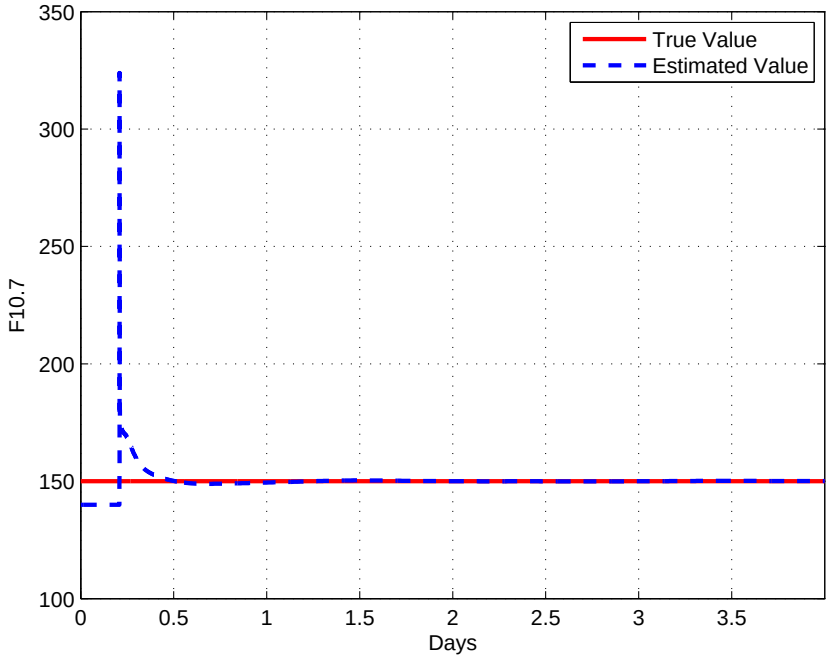

Figure 3. True and estimated F10.7. For this simulation, the F10.7 estimate converges to the true value in less than one day.

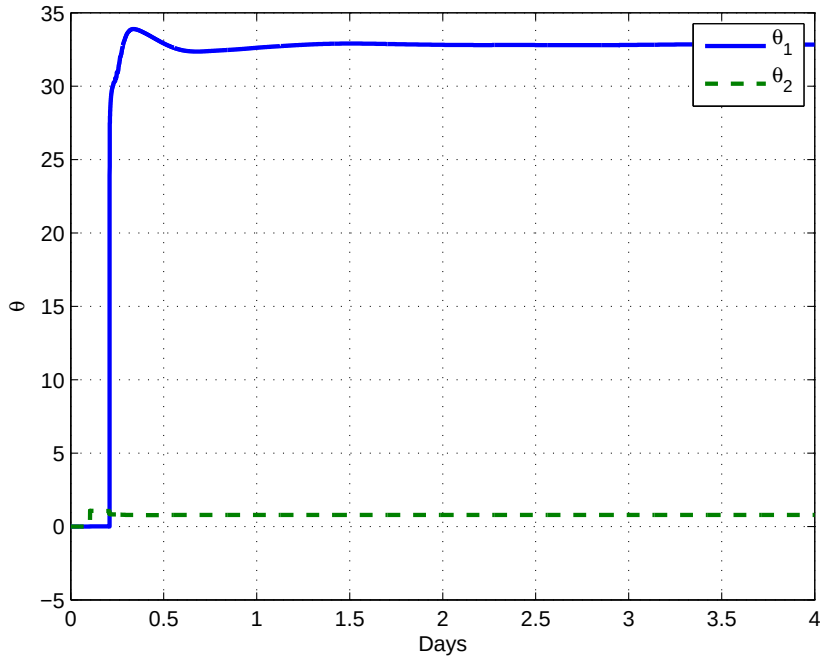

Figure 4. Estimate $\theta(k)$, which is the basis of the F10.7 estimate.

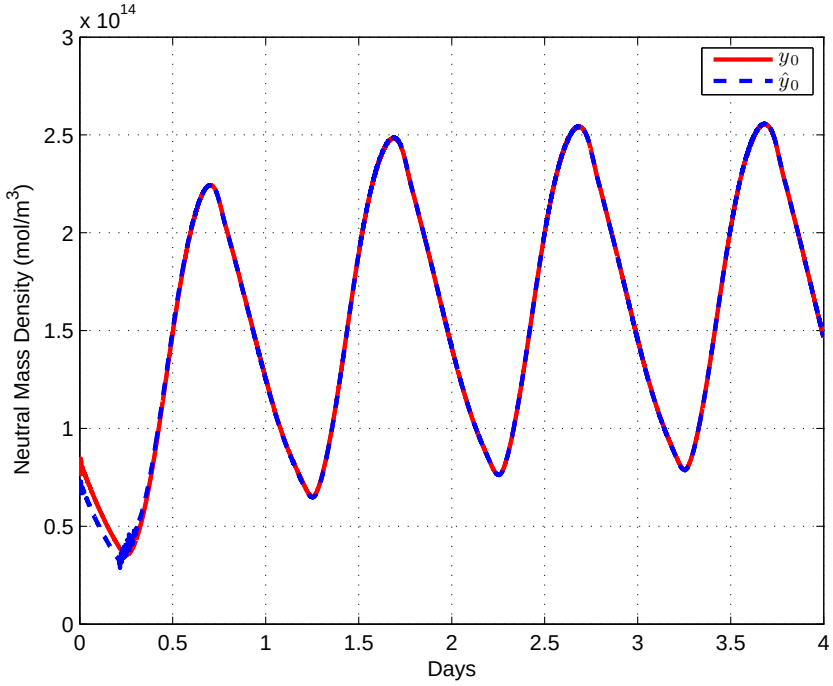

Figure 5. True and estimated neutral mass densities at an altitude of 400 km.

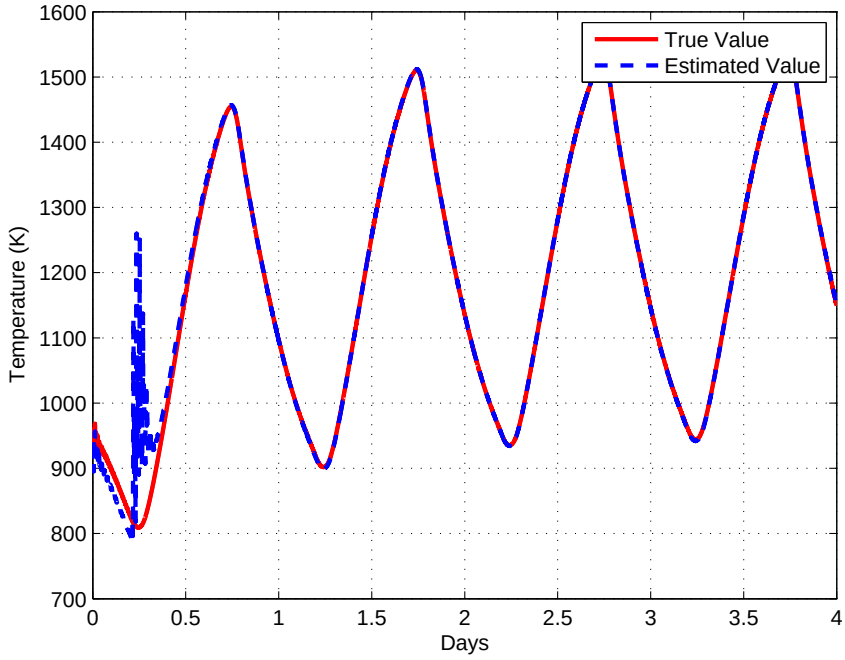

Figure 6. True and estimated temperature at the altitude of 400 km. The state estimates converge to the true values.

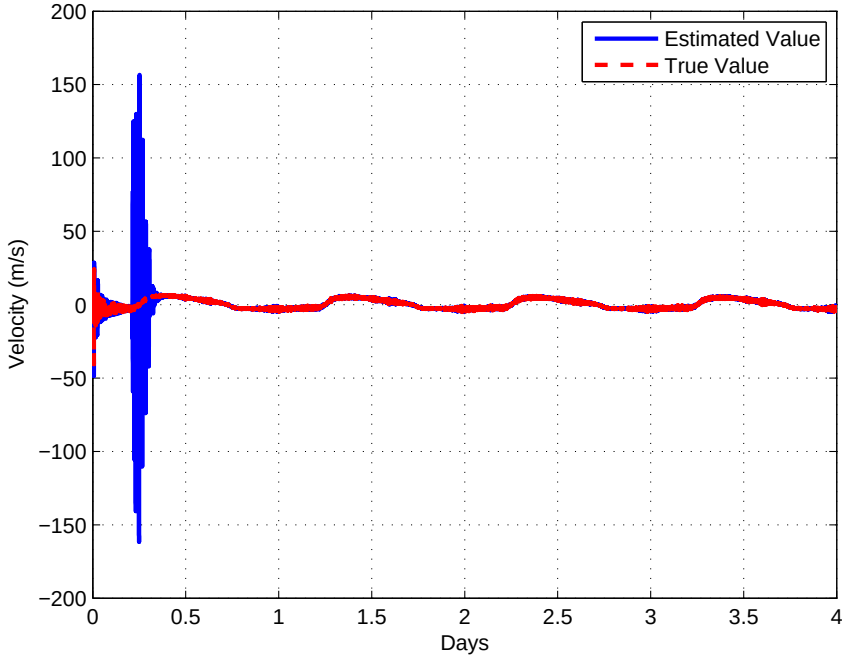

Figure 7. True and estimated velocity at the altitude of 400 km. The state estimates converge to the true values.

Next, we observe how changing saturation limits affects the estimation process. In this case, we use the initial estimate of F10.7=140. Also, the same RCASE parameters are used as in the previous example. Figures 8, 9 and 10 show simulations using saturation limits of 120/180, 125/175, and 130/170, respectively. It is evident that as we set closer limits, the time taken for the estimate to converge to the true value is significantly reduced.

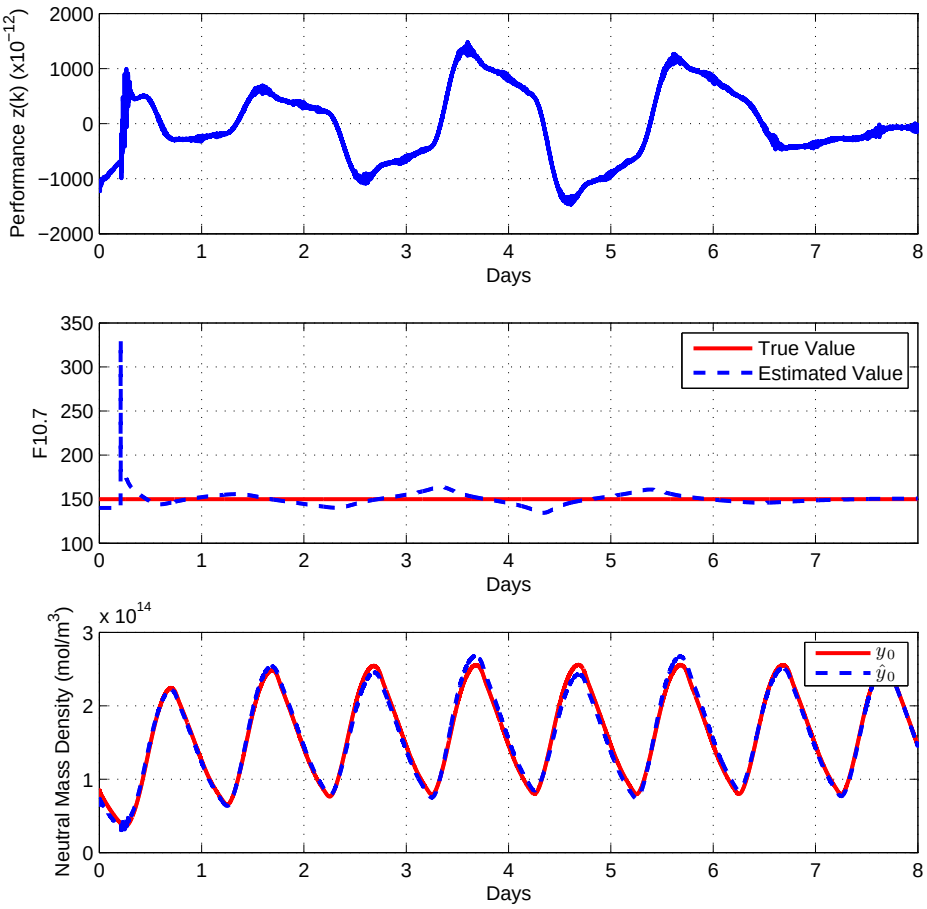

Figure 8. F10.7 estimation with saturation limits set at 120/180.

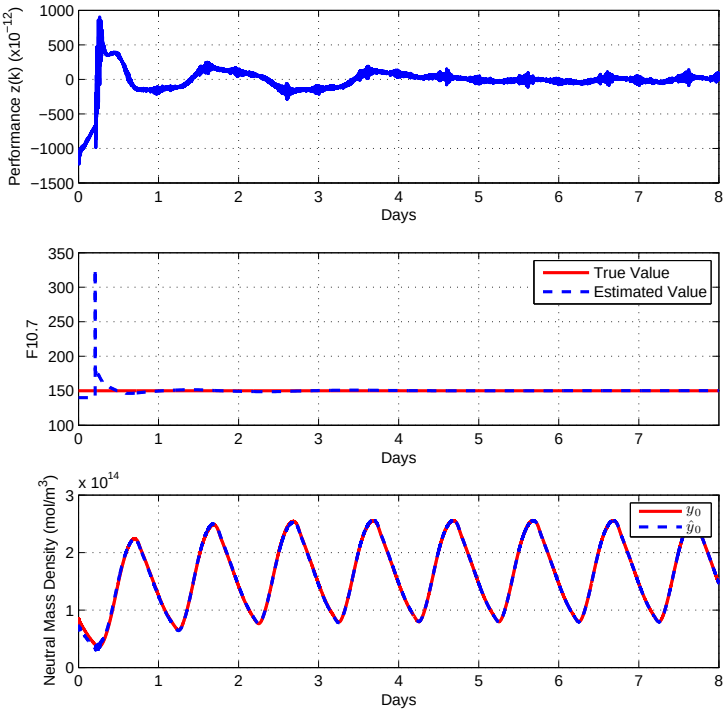

Figure 9. F10.7 estimation with saturation limits set at 125/175.

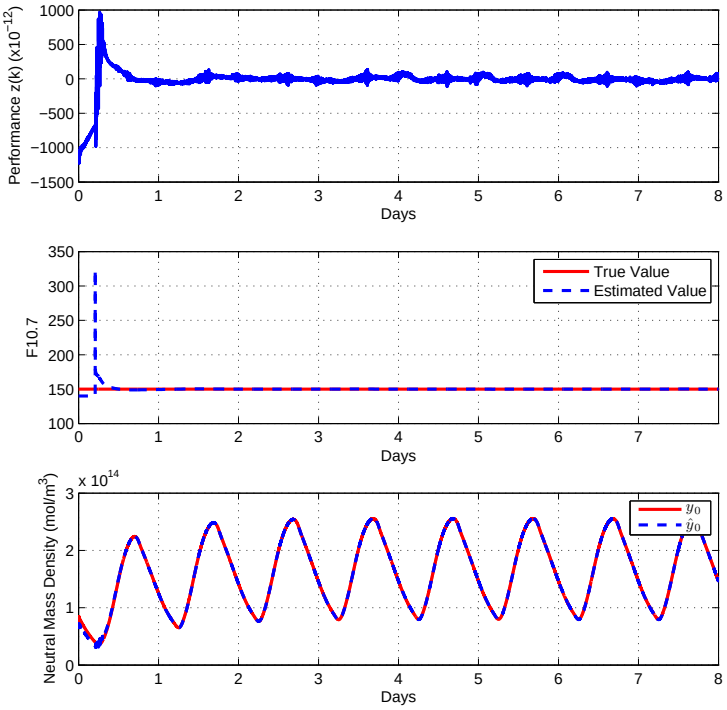

Figure 10. F10.7 estimation with saturation limits set at 130/170.

We now estimate F10.7 using the same RCASE parameters as in the previous example, but with different initial estimates. As shown in Figures 11 - 13, the estimation process takes longer to converge to the true F10.7. In the case of Figure 14, we see that the estimate does not converge to the true value of F10.7.

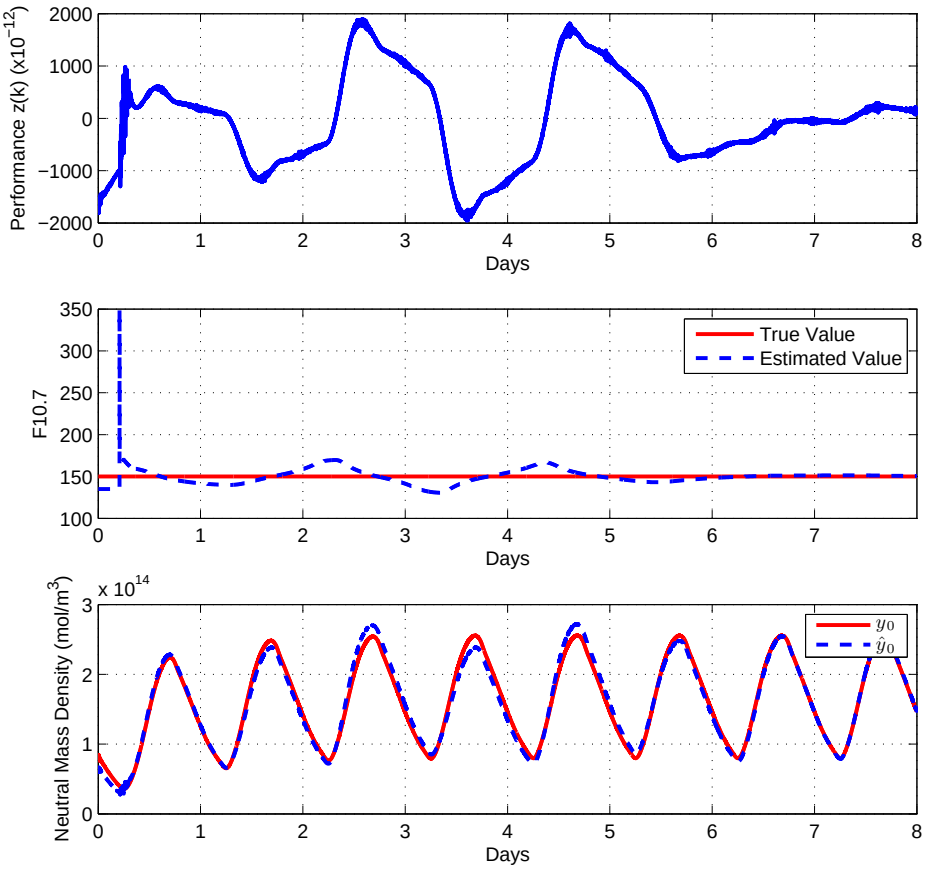

Figure 11. F10.7 estimation with initial estimate of 135.

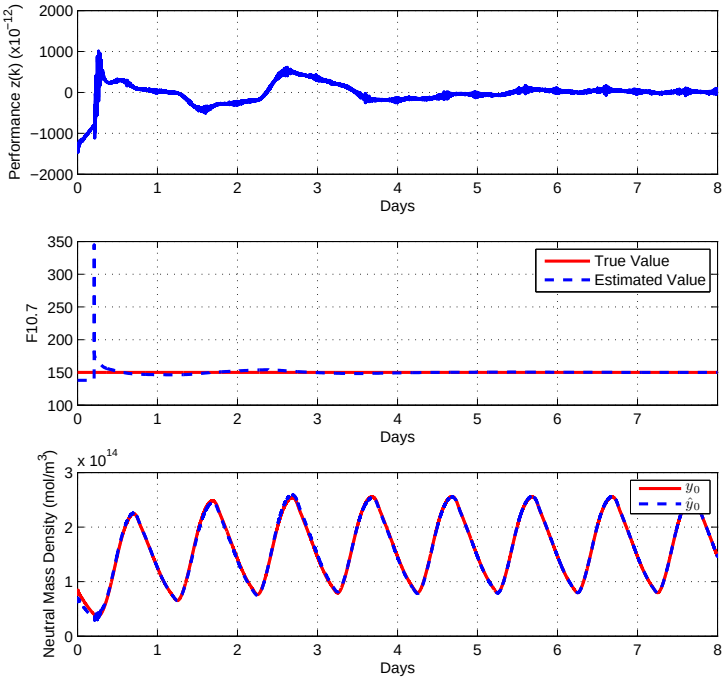

Figure 12. F10.7 estimation with initial estimate of 138.

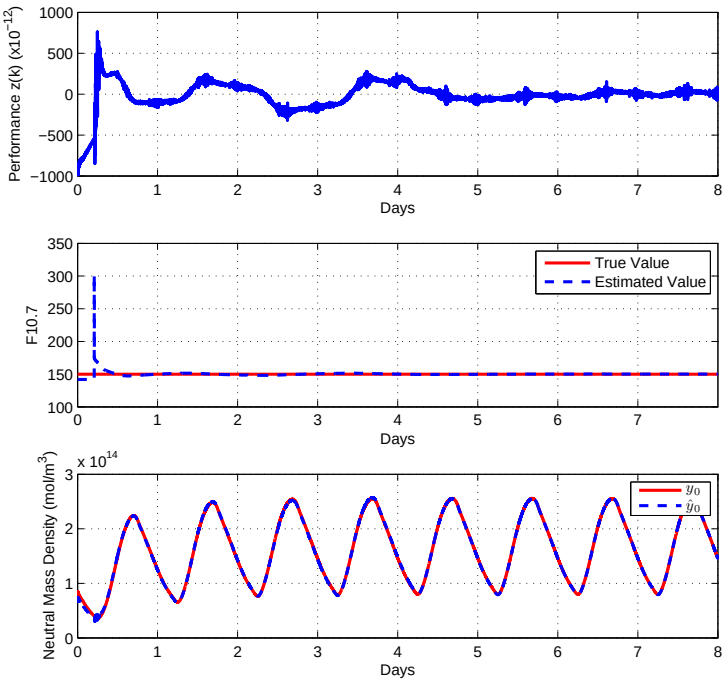

Figure 13. F10.7 estimation with initial estimate of 142.

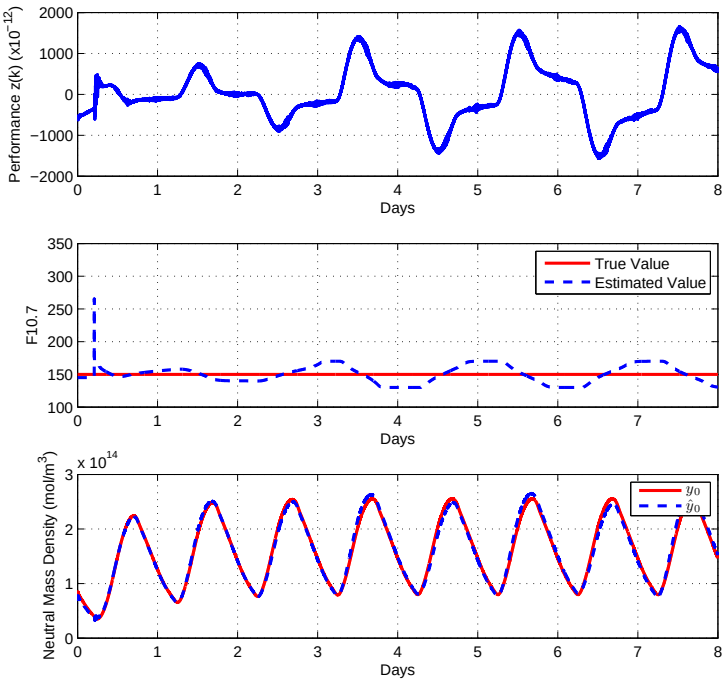

Figure 14. F10.7 estimation with initial estimate of 145.

However, by tuning the RCASE parameters, we can influence the convergence. The modified RCASE parameters in this case are set at $n_c = 1$, $\tilde{H} = 100$, $\bar{\eta} = 0$, and $\gamma = 0.02$. Also, in this case RCASE is activated after 5000 time steps. In Figures 15 - 19, we compare the estimates obtained using the parameters from the previous example with the estimates obtained using the modified parameters. As shown in Figure 16, the F10.7 estimate converges to its true value within five simulation days with the tuned parameters.

VI. Conclusions

In this paper we demonstrated input reconstruction and state estimation by estimating F10.7 and two physical states at a given location and altitude in the Global Ionosphere Thermosphere Model. We used one copy of GITM as the truth model, and another copy as the data assimilation model, which was given an incorrect initial F10.7 value. We then used RCASE to estimate the correct value of F10.7 using neutral mass density measurements from both models. We also showed that RCASE performs better under smaller saturation limits, and is able to perform reasonably well for a small range of initial estimates of F10.7 for a given set of tuning parameters. Future work will aim at reducing the requirement for tuning RCASE for different initial estimates as well as allowing it to perform well with wider saturation bounds. Extensions to 3D GITM will also be addressed.

References

[1]S. Bhattacharyya, "Observer design for linear systems with unknown inputs," *IEEE Trans. Autom. Control*, Vol. 23(3), pp. 483–484, Jun. 1978.

[2]P. K. Kitanidis, "Unbiased minimum-variance linear state estimation," *Automatica*, Vol. 23(6), pp. 775–778, Nov. 1987.

[3]M. Hou and P. Muller, "Design of observers for linear systems with unknown inputs," *IEEE Trans. Autom. Control*, Vol. 37(6), pp. 871–875, Jun. 1992.

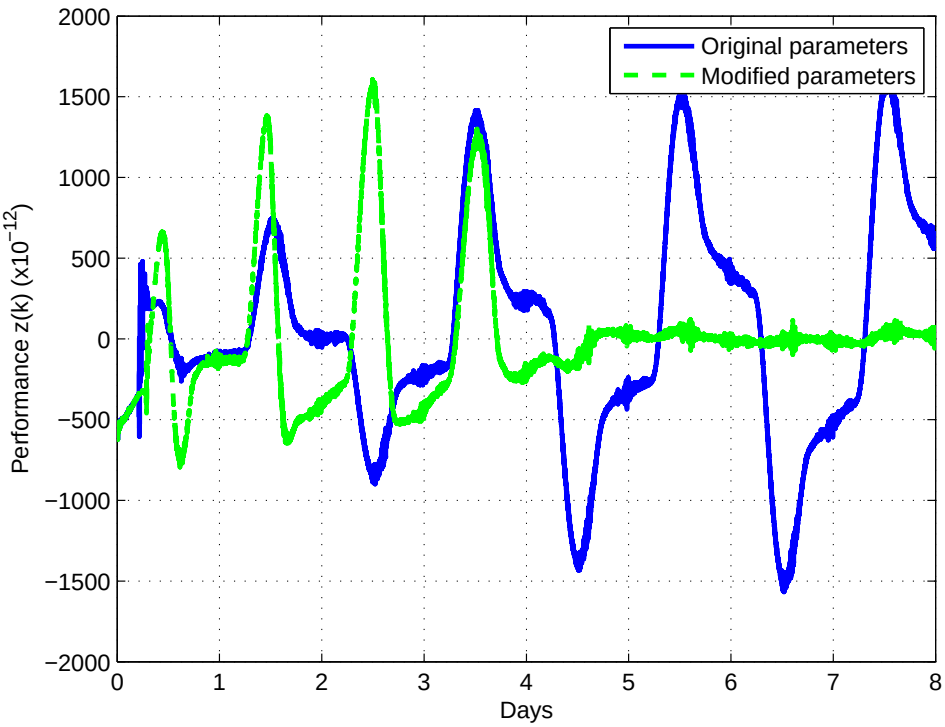

Figure 15. Comparison of performance $z(k)$ in simulations run using original parameters and modified parameters. The initial F10.7 estimate is 145.

[4]M. E. Valcher, "State observers for discrete-time linear systems with unknown inputs," *IEEE Trans. Autom. Control*, Vol. 44(2), pp. 397–401, Feb. 1999.

[5]Y. Xiong and M. Saif, "Unknown disturbance inputs estimation based on a state functional observer design," *Automatica*, Vol. 39(8), pp. 1389–1398, Aug. 2003.

[6]T. Floquet and J. P. Barbot, "State and unknown input estimation for linear discrete-time systems," *Automatica*, Vol. 42(11), pp. 1883–1889, Nov. 2006.

[7]S. Sundaram and C. N. Hadjicostis, "Delayed observers for linear systems with unknown inputs," *IEEE Trans. Autom. Control*, Vol. 52(2), pp. 334–339, Feb. 2007.

[8]H. J. Palanthandalam-Madapusi and D. S. Bernstein, "Unbiased minimum-variance filtering for input reconstruction," *IEEE American Control Conference*, pp. 5712–5717, New York, NY, Jul. 2007.

[9]D. Angeli, "A Lyapunov approach to incremental stability properties," *IEEE Trans. Autom. Control*, Vol. 47(3), pp. 410–421, Mar. 2002.

[10]G. Russo, M. di Bernardo, and E. D. Sontag, "Global Entrainment of Transcriptional Systems to Periodic Inputs," *PLOS Computational Biology*, Vol. 6(4), pp. 1–26, Apr. 2010.

[11]E. D. Sontag, "Contractive systems with inputs," *Perspectives in Mathematical Systems Theory, Control, and Signal Processing, J. C. Willems, Editor*, pp. 217–228, 2010.

[12]10.7cm Solar Radio Flux, *http://www.nwra.com/spawx/f10.html*.

[13]A. M. D'Amato, J. Springmann, A. A. Ali, J. W. Cutler, A. J. Ridley, and D. S. Bernstein, "Adaptive State Estimation for Nonminimum-Phase Systems with Uncertain Harmonic Inputs," *AIAA Guid. Nav. Contr. Conf., Portland, OR*, AIAA 2011–6315, Aug. 2011.

[14]E. Yigit and A. J. Ridley, "Effects of high-latitude thermosphere heating at various scale sizes simulated by a nonhydrostatic global thermosphere-ionosphere model," *J Atmos Sol-Terr Phys*, Vol. 73(5-6), pp. 592–600, Apr. 2011.

[15]R. G. Roble, E. C. Ridley, A. D. Richmond, and R. E. Dickinson, "A coupled thermosphere/ionosphere general circulation model," *J Geophys Res Lett*, Vol. 15(12), pp. 1325–1328, Nov. 1988.

[16]T. J. Fuller-Rowell and D. Rees, "A three-dimensional time-dependent global model of the thermosphere," *J Atmos Sci*, Vol. 37, pp. 2545–2567, Nov. 1980.

[17]Y. Deng, A. D. Richmond, A. J. Ridley, and H. L. Liu, "Assessment of the non-hydrostatic effect on the upper atmosphere using a general circulation model (GCM)," *Geophys Res Lett*, Vol. 35, L01104, 2008.

[18]A. J. Ridley, Y. Deng, and G. T'oth, "The global ionosphere-thermosphere model," *J Atmos Sol-Terr Phys*, Vol. 68(8), pp. 839–864, May 2006.

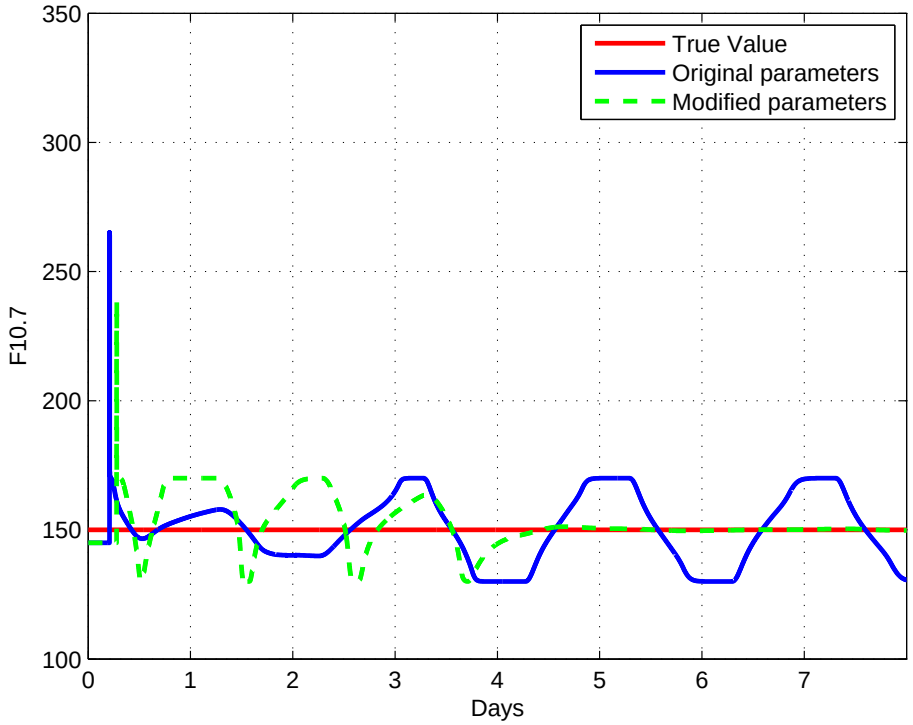

Figure 16. Comparison of F10.7 estimates in simulations using the original and modified parameters. With the modified parameters, the F10.7 estimate converges to the true value within five simulation days.

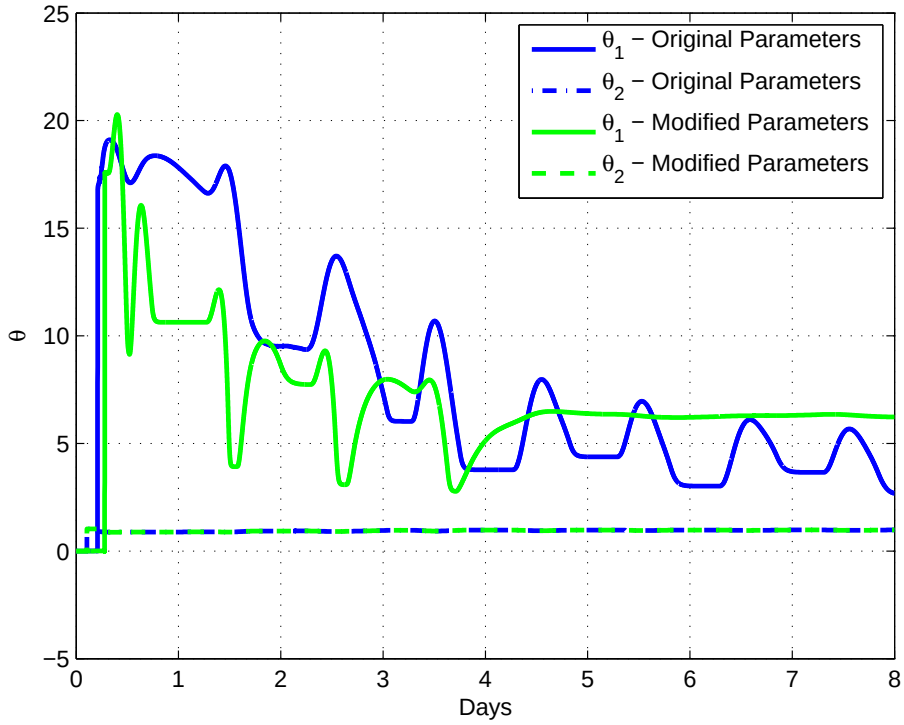

Figure 17. Comparison of $\theta(k)$ in simulations using the original and modified parameters.

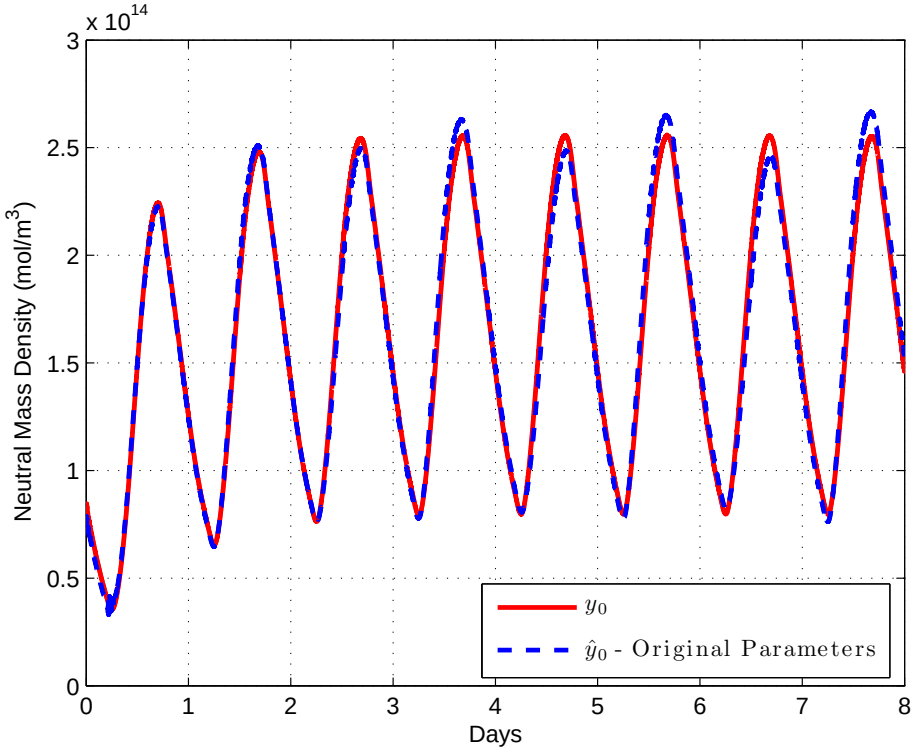

Figure 18. True and estimated Neutral Mass Density at an altitude of 400 km in a simulation using the original parameters.

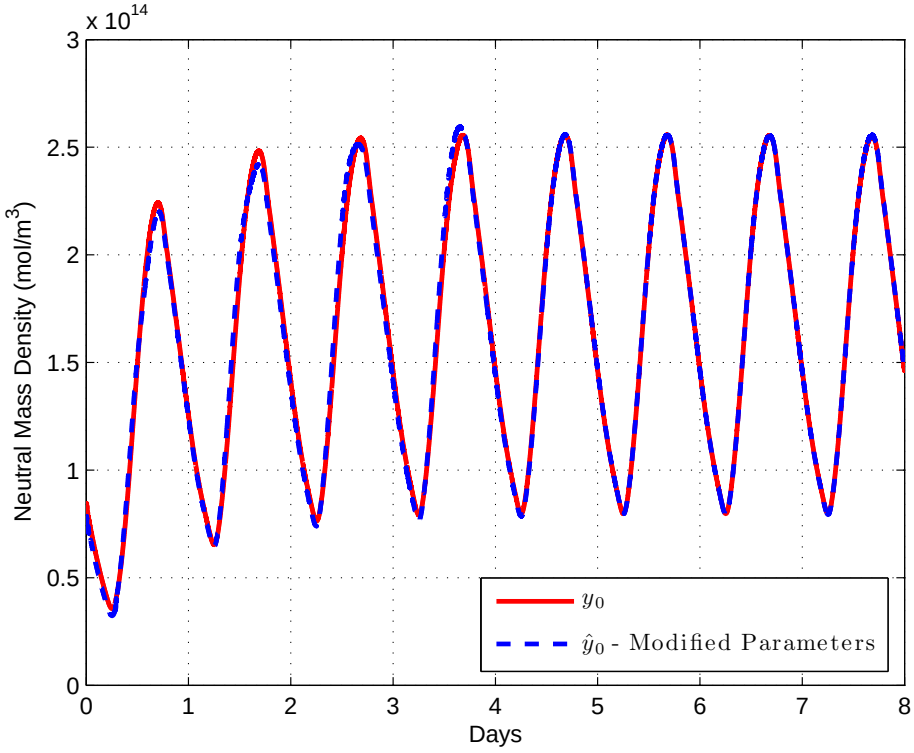

Figure 19. True and estimated Neutral Mass Density at an altitude of 400 km in a simulation using the modified parameters.